Progress In Electromagnetics Research B, Vol. 2, 83–102, 2008

A NUMERICAL ANALYSIS OF STOP BAND CHARACTERISTICS BY MULTILAYERED DIELECTRIC GRATINGS WITH SINUSOIDAL PROFILE

T. Suyama, Y. Okuno, A. Matsushima, and M. Ohtsu

Graduate School of Science and Technology
Kumamoto University
2-39-1 Kurokami Kumamoto, 860-8555 Japan

Abstract—An effective computational method based on a conventional modal expansion approach is presented for handling a multilayered dielectric grating whose profiles are multilayered and sinusoidally modulated. This structure fabricated by dielectric material is one of the useful photonic crystals. The method is based on Yasuura's modal expansion, which is known as a least-squares boundary residual method or a modified Rayleigh method. In the extended method, each layer is divided into shallow horizontal layers. The Floquet modal functions and approximate solutions are defined in each shallow layer, and the latter are matched with boundary conditions in the least-squares sense. A huge-sized least-squares problem that appears in finding the modal coefficients is solved by the QR decomposition accompanied by sequential accumulation. This procedure makes it possible to treat the case where the groove depths are the same as or a little more than the grating period. As numerical example, we calculate a diffractive characteristic by a multilayered deep dielectric grating and confirm that a common band gap occurs for both polarizations.

1. INTRODUCTION

A photonic crystal [1–3], which is composed by arraying periodically dielectric material having different permittivity, is receiving much attention nowadays. This type of crystal has a characteristic of what is called photonic band gap, which suppresses propagation in certain wavelength ranges dominated by crystal structure, and has many applications as devices for optical integrated circuits. Recent development of microfabrication technique makes it possible to produce deep gratings whose profile is strongly modulated.

From the viewpoint of numerical analysis, there are few examples which analyze diffraction characteristics of three-dimensional photonic crystals. The three-dimensional photonic crystal which we treat in the present paper is fabricated by laminating deep grating layers. To elucidate a characteristic of such photonic crystal, and to design a crystal having a desired gap, it is necessary to examine an interaction with structure (a laminate of doubly periodic deep gratings) and light (an electromagnetic wave). It is expected that the stop band characteristic is appeared clearly by a multilayered grating, and the polarization dependence is decreased by an introduction of two-dimensional periodicity. We analyze the problem of plane wave diffraction by the multilayered deep grating, and confirm that a characteristic as photonic crystal is provided.

In order to examine the properties of photonic crystals from such a point of view, we aimed at establishing technique to analyze a diffraction of an electromagnetic wave by the multilayered deep grating with high accuracy. We use Yasuura's method (mode-matching method) [4–8] as a numerical tool, which is one of the excellent techniques for solving the problem of diffraction by gratings. Although alternative terminology for this method (e.g., a least-squares boundary residual method [9] or a modified Rayleigh method [10]) exists, we employ the name throughout this paper. When modulation of a grating profile is weak, e.g., the depth-to-period ratio does not exceed 0.5, we can obtain the diffracted field with high accuracy by using the method. When the profile is strongly deformed, however, the method fails to find precise solutions. It is an accepted knowledge that the conventional Yasuura's method (CYM) [4–8] with Floquet modes as basis functions does not have a wide range of application [10, 11].

In order to overcome the difficulty above, we employ a technique of extending the range of application of CYM, which was successfully applied to a nonlaminated deep grating [12]. First, we partition the entire plane into $L + 1$ layers as usual, where L is the number of dielectric layers including a substrate. In addition to this conventional partition, each layer is further divided into shallow horizontal layers. Second, we define approximate solutions in each region in the form of truncated modal expansions with unknown coefficients. The solutions are matched with boundary conditions in the least-squares sense. This extended and accurate treatment, however, faces a huge-sized least-squares problem. We, hence, introduce a sequential accumulation which enables us to find the unknown modal coefficients in an iterative manner and reduces the storage space requirement and CPU time in numerical computations.

2. FORMULATION OF THE PROBLEM

We formulate a problem of diffraction from a multilayered doubly periodic gratings when an electromagnetic plane wave is incident on the multilayered grating. A time factor $\exp(-i\omega t)$ is suppressed throughout this paper.

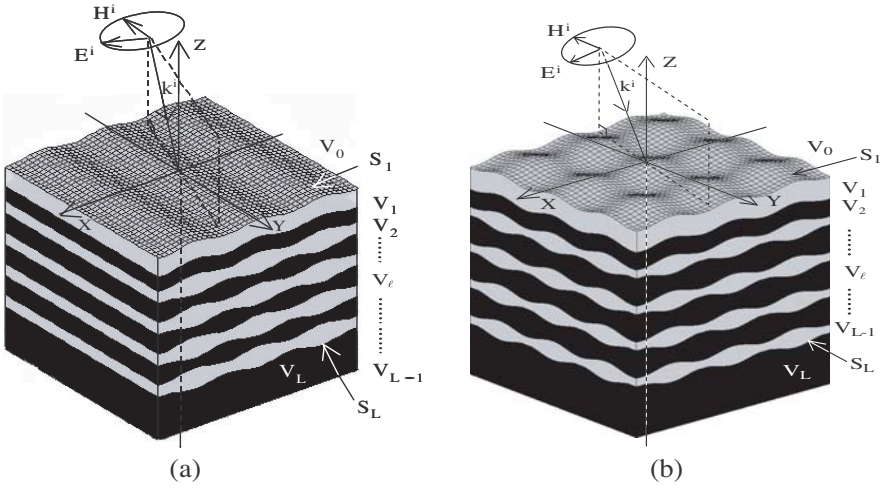

Figure 1. Multilayered sinusoidal dielectric gratings. (a) Singly periodic. (b) Doubly periodic.

2.1. Geometry of the Gratings

Figure 1 shows the structure of multilayered dielectric gratings with (a) single and (b) doubly periodicity. The multilayered grating which is laminating $L-1$ grating layers has period D in X-direction for (a) and in both X- and Y-directions for (b). The semi-infinite region over the multilayered grating and the substrate are denoted by V_0 and V_L, respectively. Moreover, each region inside the multilayered grating, which is numbered starting from the incident side, is denoted by V_ℓ ($\ell = 1, 2, \ldots, L-1$). The regions V_ℓ ($\ell = 0, 1, \ldots, L$) are filled with isotropic and homogeneous media with refractive indices n_ℓ, and a permeability of each region is equal with that of the air μ_0. The interface between $\mathrm{V}_{\ell-1}$ and V_ℓ is denoted by S_ℓ ($\ell = 1, 2, \ldots, L$).

The profile of S_ℓ is sinusoidal and given by

$$z = \eta_\ell(x,y) = \begin{cases} H_\ell \cos\left(\dfrac{2\pi x}{D} + p_\ell\right) - \displaystyle\sum_{i=1}^{\ell-1} w_i & \text{(Fig. 1(a))} \\ \dfrac{H_\ell}{2}\left\{\cos\left(\dfrac{2\pi x}{D}+p_\ell\right)+\cos\left(\dfrac{2\pi y}{D}+p_\ell\right)\right\} - \displaystyle\sum_{i=1}^{\ell-1} w_i & \text{(Fig. 1(b))} \end{cases} \quad (1)$$

where p_ℓ stands for the phase of S_ℓ in each direction, and w_ℓ denotes an average distance between S_ℓ and $S_{\ell+1}$. The value H_ℓ is regarded as a groove depth of the boundary S_ℓ.

It is pointed out that we can easily generalize the shape of S_ℓ by distinguishing D and p_ℓ between X- and Y-directions, say, by writing as D_x, D_y, $p_{x\ell}$, and $p_{y\ell}$. A singly periodic grating is an special case where $D_y \to \infty$ in a doubly periodic one. In the present paper, we concentrate our attention to describing the analysis only for doubly periodic case, since it reduces to another case through a simple procedure.

2.2. Incident Wave

The electric and magnetic fields of an incident wave are given by

$$\begin{pmatrix} \boldsymbol{E}^{\mathrm{i}} \\ \boldsymbol{H}^{\mathrm{i}} \end{pmatrix}(\mathrm{P}) = \begin{pmatrix} \boldsymbol{e}^{\mathrm{i}} \\ \boldsymbol{h}^{\mathrm{i}} \end{pmatrix} \exp(i\boldsymbol{k}^{\mathrm{i}} \cdot \boldsymbol{P}) \quad (2)$$

with

$$\boldsymbol{h}^{\mathrm{i}} = (1/\omega\mu_0)\boldsymbol{k}^{\mathrm{i}} \times \boldsymbol{e}^{\mathrm{i}} \quad (3)$$

Here, $\boldsymbol{P}$ is a position vector for an observation point P(X, Y, Z), and $\boldsymbol{k}^{\mathrm{i}}$ is the wave vector of incident wave defined by

$$\boldsymbol{k}^{\mathrm{i}} = [\alpha, \beta, -\gamma]^{\mathrm{T}} \quad (4)$$

where $\alpha = n_0 k \sin\theta\cos\phi$, $\beta = n_0 k \sin\theta\sin\phi$, $\gamma = n_0 k\cos\theta$. The symbol k ($= 2\pi/\lambda$) is the wave number in vacuum, and λ is a wavelength of incident wave. We define θ and ϕ as polar and azimuth angles, respectively, as shown in Fig. 2(a), and the superscript "T" denotes a transposition.

The amplitude of incident electric field is decomposed into TE-

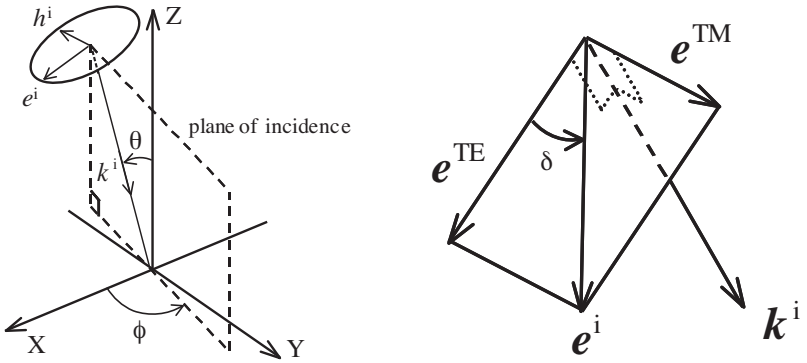

Figure 2. An incident plane wave. (a) Polar and azimuth angles. (b) Polarization angle.

and TM-modes (to the Z-axis) [13]. It is written as

$$\boldsymbol{e}^{\mathrm{i}} = \cos\delta \boldsymbol{e}^{\mathrm{TE}} + \sin\delta \boldsymbol{e}^{\mathrm{TM}} \tag{5}$$

$$\boldsymbol{e}^{\mathrm{TE}} = [\sin\phi, -\cos\phi, 0]^{\mathrm{T}} \tag{6}$$

$$\boldsymbol{e}^{\mathrm{TM}} = [\cos\theta\cos\phi, \cos\theta\sin\phi, \sin\theta]^{\mathrm{T}} \tag{7}$$

Here, the superscript TE (TM) means the absence of Z component of an electric (magnetic) field. The symbol δ is a polarization angle between $\boldsymbol{e}^{\mathrm{TE}}$ and $\boldsymbol{e}^{\mathrm{i}}$ as shown in Fig. 2(b); it shows TE-mode (TM-mode) incidence in case of $\delta = 0^\circ$ ($\delta = 90^\circ$).

2.3. Diffracted Wave

We denote the diffracted fields by $\boldsymbol{E}_\ell(\mathrm{P})$ and $\boldsymbol{H}_\ell(\mathrm{P})$ in the region V_ℓ ($\ell = 0, 1, \ldots, L$). They satisfy following conditions:

- The Helmholtz equation:

$$(\nabla^2 + n_\ell^2 k^2) \begin{pmatrix} \boldsymbol{E}_\ell \\ \boldsymbol{H}_\ell \end{pmatrix} (\mathrm{P}) = 0 \quad (\ell = 0,\, 1,\, \ldots,\, L) \tag{8}$$

- A radiation condition:
  $\boldsymbol{E}_0$ and $\boldsymbol{H}_0$ propagate or attenuate in the positive Z-direction.
  $\boldsymbol{E}_L$ and $\boldsymbol{H}_L$ propagate or attenuate in the negative Z-direction.
- A periodicity condition:

$$f(X + D,\, Y,\, Z) = \exp(i\alpha D) f(X,\, Y,\, Z) \tag{9}$$

$$f(X,\, Y + D,\, Z) = \exp(i\beta D) f(X,\, Y,\, Z) \tag{10}$$

Here, f denotes any component of $\boldsymbol{E}_\ell(\mathrm{P})$ or $\boldsymbol{H}_\ell(\mathrm{P})$.

- A boundary condition ($0 < X < D$, $0 < Y < D$; $\ell = 1, 2, \ldots, L$):

$$\boldsymbol{\nu} \times \left[\begin{pmatrix} \boldsymbol{E}_{\ell-1} \\ \boldsymbol{H}_{\ell-1} \end{pmatrix} + \delta_{\ell 1} \begin{pmatrix} \boldsymbol{E}^{\mathrm{i}} \\ \boldsymbol{H}^{\mathrm{i}} \end{pmatrix} - \begin{pmatrix} \boldsymbol{E}_{\ell} \\ \boldsymbol{H}_{\ell} \end{pmatrix} \right] = 0 \ (\text{on } \mathrm{S}_\ell) \quad (11)$$

where $\delta_{\ell 1}$ is Kronecker's delta, and $\boldsymbol{\nu}$ denotes the unit normal vector on the surface S_ℓ, which is given by

$$\boldsymbol{\nu} = \frac{\left(-\dfrac{\partial \eta_\ell(x,y)}{\partial x}, -\dfrac{\partial \eta_\ell(x,y)}{\partial y}, 1 \right)}{\sqrt{\left(\dfrac{\partial \eta_\ell(x,y)}{\partial x} \right)^2 + \left(\dfrac{\partial \eta_\ell(x,y)}{\partial y} \right)^2 + 1}} \quad (12)$$

2.4. Divisions of the Grating

If a groove depth H_ℓ is small enough compared with a period D, we can obtain a solution with enough accuracy when applying Yasuura's method directly to the problem shown in Fig. 1 [14, 15]. In this case, however, we hardly achieve high accuracy when the depth is deep. The technique of extending the range of application has been used for solving the problem of diffraction by one-dimensional nonlaminated deep grating [12]. The present section applies this method to two-dimensional and multilayered grating.

We first define a fictitious flat layer between the bottom of $\mathrm{S}_{\ell-1}$ ($Z = \min \eta_{\ell-1}$) and the top of S_ℓ ($Z = \max \eta_\ell$) as U_0^ℓ ($\ell = 2, 3, \ldots, L$). In the same way, L_0^ℓ is a layer between the bottom of S_ℓ and the top of $\mathrm{S}_{\ell+1}$ ($\ell = 1, 2, \ldots, L-1$). Note that U_0^ℓ=$\mathrm{L}_0^{\ell-1}$ and L_0^ℓ=$\mathrm{U}_0^{\ell+1}$. The semi infinite space over the top of S_1 (under the bottom of S_L) is denoted as U_0^1 (L_0^L). We next slice each groove region ($\min \eta_\ell < Z < \max \eta_\ell$) into $2Q$ sections U_q^ℓ and L_q^ℓ ($q = 1, 2, \ldots, Q$), which are located in the upper and lower sides of the grating surface S_ℓ, respectively, as shown in Fig. 3.

After all, we have a couple of semi infinite regions (U_0^1 and L_0^L), $L-1$ slab regions (U_0^ℓ and L_0^ℓ), and $2LQ$ sections which divide L groove regions. These divisions are described as

$$\mathrm{U}_0^1 = \{\mathrm{P};\ Z > z_0^1\} \quad (13)$$

$$\mathrm{L}_0^L = \{\mathrm{P};\ Z < z_Q^L\} \quad (14)$$

$$\mathrm{U}_0^\ell = \{\mathrm{P};\ z_Q^{\ell-1} > Z > z_0^\ell\} \quad (\ell = 2, 3, \ldots, L) \quad (15)$$

$$\mathrm{L}_0^\ell = \{\mathrm{P};\ z_0^{\ell+1} < Z < z_Q^\ell\} \quad (\ell = 1, 2, \ldots, L-1) \quad (16)$$

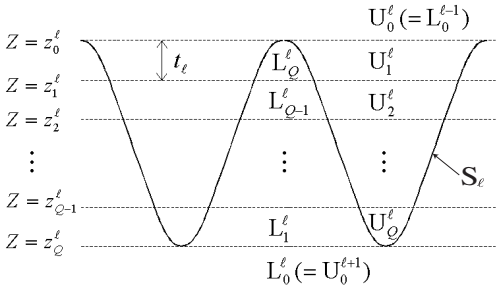

Figure 3. Partition of the ℓ-th grating region.

$$\begin{aligned} \mathrm{U}_q^\ell &= \{\mathrm{P};\ z_{q-1}^\ell > Z > z_q^\ell\ ,\ Z > \eta_\ell(x,y)\} \\ &\quad (\ell = 1,2,\ldots,L;\ q = 1,2,\ldots,Q) \end{aligned} \tag{17}$$

$$\begin{aligned} \mathrm{L}_q^\ell &= \{\mathrm{P};\ z_{Q-q+1}^\ell < Z < z_{Q-q}^\ell\ ,\ Z < \eta_\ell(x,y)\} \\ &\quad (\ell = 1,2,\ldots,L;\ q = 1,2,\ldots,Q) \end{aligned} \tag{18}$$

where

$$z_q^\ell = H_\ell - qt_\ell - \sum_{i=1}^{\ell-1} w_i,\ t_\ell = \frac{2H_\ell}{Q}\ (\ell = 1,2,\ldots,L;\ q = 0,1,\ldots,Q) \tag{19}$$

with regarding as $z_{-1}^1 = \infty$ and $z_{Q+1}^L = -\infty$.

The diffracted fields in sub-region R_q^ℓ (R = U, L) are denoted by $\boldsymbol{E}^{\mathrm{R}_q^\ell}$, $\boldsymbol{H}^{\mathrm{R}_q^\ell}$ (ℓ = 1, 2, ... , L; q = 0, 1, ... , Q). These fields should satisfy the boundary condition (11) as well as an additional set of boundary conditions on the fictitious boundaries ($Z = z_q^\ell$):

$$\boldsymbol{i}_Z \times \left[\begin{pmatrix} \boldsymbol{E}^{\mathrm{R}_q^\ell} \\ \boldsymbol{H}^{\mathrm{R}_q^\ell} \end{pmatrix} + \delta_{\ell 1}\delta_{q0} \begin{pmatrix} \boldsymbol{E}^{\mathrm{i}} \\ \boldsymbol{H}^{\mathrm{i}} \end{pmatrix} - \begin{pmatrix} \boldsymbol{E}^{\mathrm{R}_{q+1}^\ell} \\ \boldsymbol{H}^{\mathrm{R}_{q+1}^\ell} \end{pmatrix} \right] = 0 \tag{20}$$

$$(0 < X < D,\ \ 0 < Y < D;\ \ell = 1,\ 2,\ \ldots,\ L;\ q = 0,\ 1,\ \ldots,\ Q-1)$$

Here, $\boldsymbol{i}_Z$ is a unit normal vector in the Z-direction.

3. YASUURA'S METHOD

Now, we explain Yasuura's method for finding the diffracted fields by the multilayered doubly periodic deep grating. We introduce the vector modal functions in the region V_ℓ (ℓ = 0, 1, ... , L) to express

the diffracted fields in each divided region. To construct the wave functions $\boldsymbol{E}_N^{\mathrm{R}_q^\ell}(\mathrm{P})$ and $\boldsymbol{H}_N^{\mathrm{R}_q^\ell}(\mathrm{P})$, we define the electric modal function $\boldsymbol{\varphi}_{\ell mn}^{\mathrm{TE,TM}\pm}(\mathrm{P})$ and the magnetic modal function $\boldsymbol{\psi}_{\ell mn}^{\mathrm{TE,TM}\pm}(\mathrm{P})$ by

$$\boldsymbol{\varphi}_{\ell mn}^{\mathrm{TE,TM}\pm}(\mathrm{P}) = \boldsymbol{e}_{\ell mn}^{\mathrm{TE,TM}\pm}\phi_{\ell mn}^{\pm}(\mathrm{P}) \tag{21}$$

$$\boldsymbol{e}_{\ell mn}^{\mathrm{TE}\pm} = \frac{\boldsymbol{k}_{\ell mn}^{\pm}\times\boldsymbol{i}_Z}{|\boldsymbol{k}_{\ell mn}^{\pm}\times\boldsymbol{i}_Z|}, \quad \boldsymbol{e}_{\ell mn}^{\mathrm{TM}\pm} = \frac{\boldsymbol{e}_{\ell mn}^{\mathrm{TE}\pm}\times\boldsymbol{k}_{\ell mn}^{\pm}}{|\boldsymbol{e}_{\ell mn}^{\mathrm{TE}\pm}\times\boldsymbol{k}_{\ell mn}^{\pm}|} \tag{22}$$

$$\boldsymbol{\psi}_{\ell mn}^{\mathrm{TE,TM}\pm}(\mathrm{P}) = \frac{1}{\omega\mu_0}\boldsymbol{k}_{\ell mn}^{\pm}\times\boldsymbol{\varphi}_{\ell mn}^{\mathrm{TE,TM}\pm}(\mathrm{P}) \tag{23}$$

where $\phi_{\ell mn}^{\pm}(\mathrm{P})$ is a separated solution of the Helmholtz equation satisfying the periodic condition in region V_ℓ ($\ell = 0, 1, \ldots, L$). It is written by

$$\phi_{\ell mn}^{\pm}(\mathrm{P}) = \exp(i\boldsymbol{k}_{\ell mm}^{\pm}\cdot\boldsymbol{P}) \quad (m, n = 0, \pm1, \pm2, \ldots) \tag{24}$$

where the upper and lower signs go together, and $\boldsymbol{k}_{\ell mn}^{\pm}$ is the wave vector of the (m, n)-th order diffracted wave given by

$$\boldsymbol{k}_{\ell mn}^{\pm} = [\alpha_m, \beta_n, \pm\gamma_{\ell mn}]^{\mathrm{T}} \tag{25}$$

$$\alpha_m = \alpha + \frac{2m\pi}{D}, \quad \beta_n = \beta + \frac{2n\pi}{D} \tag{26}$$

$$\gamma_{\ell mn} = (n_\ell^2 k^2 - \alpha_m^2 - \beta_n^2)^{1/2}, \quad \mathrm{Im}(\gamma_{\ell mn}) \geq 0 \tag{27}$$

In terms of linear combinations of the vector modal functions, we form approximate wave functions for the diffracted electromagnetic fields $\boldsymbol{E}_N^{\mathrm{R}_q^\ell}(\mathrm{P})$ and $\boldsymbol{H}_N^{\mathrm{R}_q^\ell}(\mathrm{P})$ in the region R_q^ℓ ($\mathrm{R} = \mathrm{U}, \mathrm{L}$; $\ell = 1, 2, \ldots, L$; $q = 0, 1, \ldots, Q$) with the truncation number N (the number of modes is $M = 2N + 1$) as follows.

(i) In the region U_0^1 ($\mathrm{P} \in \mathrm{U}_0^1$):

$$\begin{pmatrix} \boldsymbol{E}_N^{\mathrm{U}_0^1} \\ \boldsymbol{H}_N^{\mathrm{U}_0^1} \end{pmatrix}(\mathrm{P}) = \sum_{\mathrm{W=TE,TM}} \sum_{m,n=-N}^{N} A_{1mn}^{\mathrm{W}(0)} \begin{pmatrix} \boldsymbol{\varphi}_{0mn}^{\mathrm{W}+} \\ \boldsymbol{\psi}_{0mn}^{\mathrm{W}+} \end{pmatrix}(\mathrm{P} - \boldsymbol{i}_Z z_0^1) \tag{28}$$

(ii) In the region L_0^L ($\mathrm{P} \in \mathrm{L}_0^L$):

$$\begin{pmatrix} \boldsymbol{E}_N^{\mathrm{L}_0^L} \\ \boldsymbol{H}_N^{\mathrm{L}_0^L} \end{pmatrix}(\mathrm{P}) = \sum_{\mathrm{W=TE,TM}} \sum_{m,n=-N}^{N} D_{Lmn}^{\mathrm{TE}(0)} \begin{pmatrix} \boldsymbol{\varphi}_{Lmn}^{\mathrm{W}-} \\ \boldsymbol{\psi}_{Lmn}^{\mathrm{W}-} \end{pmatrix}(\mathrm{P} - \boldsymbol{i}_Z z_Q^L) \tag{29}$$

(iii) In the region L_0^ℓ $(= \mathrm{U}_0^{\ell+1})$ $(\mathrm{P} \in \mathrm{L}_0^\ell = \mathrm{U}_0^{\ell+1};\ \ell = 1, 2, \ldots, L-1)$:

$$\begin{aligned}\begin{pmatrix} \boldsymbol{E}_N^{\mathrm{L}_0^\ell} \\ \boldsymbol{H}_N^{\mathrm{L}_0^\ell} \end{pmatrix}(\mathrm{P}) &= \begin{pmatrix} \boldsymbol{E}_N^{\mathrm{U}_0^{\ell+1}} \\ \boldsymbol{H}_N^{\mathrm{U}_0^{\ell+1}} \end{pmatrix}(\mathrm{P}) \\ &= \sum_{\mathrm{W=TE,TM}} \sum_{m,n=-N}^{N} A_{\ell+1,mn}^{\mathrm{TE}(0)} \begin{pmatrix} \boldsymbol{\varphi}_{\ell mn}^{\mathrm{W}+} \\ \boldsymbol{\psi}_{\ell mn}^{\mathrm{W}+} \end{pmatrix}(\mathrm{P} - \boldsymbol{i}_Z z_0^{\ell+1}) \\ &\quad + \sum_{\mathrm{W=TE,TM}} \sum_{m,n=-N}^{N} D_{\ell mn}^{\mathrm{TE}(0)} \begin{pmatrix} \boldsymbol{\varphi}_{\ell mn}^{\mathrm{W}-} \\ \boldsymbol{\psi}_{\ell mn}^{\mathrm{W}-} \end{pmatrix}(\mathrm{P} - \boldsymbol{i}_Z z_Q^\ell) \quad (30)\end{aligned}$$

(iv) In the region U_q^ℓ $(\mathrm{P} \in \mathrm{U}_q^\ell;\ \ell = 1, 2, \ldots, L;\ q = 1, 2, \ldots, Q)$:

$$\begin{aligned}\begin{pmatrix} \boldsymbol{E}_N^{\mathrm{U}_q^\ell} \\ \boldsymbol{H}_N^{\mathrm{U}_q^\ell} \end{pmatrix}(\mathrm{P}) &= \sum_{\mathrm{W=TE,TM}} \sum_{m,n=-N}^{N} A_{\ell mn}^{\mathrm{TE}(q)} \begin{pmatrix} \boldsymbol{\varphi}_{\ell-1,mn}^{\mathrm{W}+} \\ \boldsymbol{\psi}_{\ell-1,mn}^{\mathrm{W}+} \end{pmatrix}(\mathrm{P} - \boldsymbol{i}_Z z_q^\ell) \\ &\quad + \sum_{\mathrm{W=TE,TM}} \sum_{m,n=-N}^{N} B_{\ell mn}^{\mathrm{TE}(q)} \begin{pmatrix} \boldsymbol{\varphi}_{\ell-1,mn}^{\mathrm{W}-} \\ \boldsymbol{\psi}_{\ell-1,mn}^{\mathrm{W}-} \end{pmatrix}(\mathrm{P} - \boldsymbol{i}_Z z_{q-1}^\ell) \quad (31)\end{aligned}$$

(v) In the region L_q^ℓ $(\mathrm{P} \in \mathrm{L}_q^\ell;\ \ell = 1, 2, \ldots, L;\ q = 1, 2, \ldots, Q)$:

$$\begin{aligned}\begin{pmatrix} \boldsymbol{E}_N^{\mathrm{L}_q^\ell} \\ \boldsymbol{H}_N^{\mathrm{L}_q^\ell} \end{pmatrix}(\mathrm{P}) &= \sum_{\mathrm{W=TE,TM}} \sum_{m,n=-N}^{N} C_{\ell mn}^{\mathrm{TE}(q)} \begin{pmatrix} \boldsymbol{\varphi}_{\ell mn}^{\mathrm{W}+} \\ \boldsymbol{\psi}_{\ell mn}^{\mathrm{W}+} \end{pmatrix}(\mathrm{P} - \boldsymbol{i}_Z z_{Q-q+1}^\ell) \\ &\quad + \sum_{\mathrm{W=TE,TM}} \sum_{m,n=-N}^{N} D_{\ell mn}^{\mathrm{TE}(q)} \begin{pmatrix} \boldsymbol{\varphi}_{\ell mn}^{\mathrm{W}-} \\ \boldsymbol{\psi}_{\ell mn}^{\mathrm{W}-} \end{pmatrix}(\mathrm{P} - \boldsymbol{i}_Z z_{Q-q}^\ell) \quad (32)\end{aligned}$$

Note that, though we should have represented the modal coefficients as $A_{\ell mn}^{\mathrm{TE,TM}(q)}(N)$, $B_{\ell mn}^{\mathrm{TE,TM}(q)}(N)$, $C_{\ell mn}^{\mathrm{TE,TM}(q)}(N)$, and $D_{\ell mn}^{\mathrm{TE,TM}(q)}(N)$ as a functions of the truncation number N, we omitted "(N)" for simplicity. The total number of the coefficients is $N_{\mathrm{T}} = 4L(2Q+1)(2N+1)^2$.

The above expansion coefficients are determined so that the functions $\boldsymbol{E}_N^{\mathrm{R}_q^\ell}(\mathrm{P})$ and $\boldsymbol{H}_N^{\mathrm{R}_q^\ell}(\mathrm{P})$ satisfy the boundary conditions (11) and (20) in the weighted least-squares sense. To do this, we define a mean-square error by

$$I_N = \sum_{\ell=1}^{L} \sum_{q=0}^{Q-1} \int_{\Gamma_{\ell q}^{\mathrm{U}}} \left| \boldsymbol{i}_Z \times \left[\boldsymbol{E}_N^{\mathrm{U}_q^\ell} + \delta_{\ell 1}\delta_{q0}\boldsymbol{E}^{\mathrm{i}} - \boldsymbol{E}_N^{\mathrm{U}_{q+1}^\ell} \right](\mathrm{P}) \right|^2 dS$$

$$+\sum_{\ell=1}^{L}\sum_{q=0}^{Q-1}\int_{\Gamma^{\mathrm{L}}_{\ell q}}\left|\boldsymbol{i}_Z\times\left[\boldsymbol{E}_N^{\mathrm{L}^{\ell}_{q+1}}-\boldsymbol{E}_N^{\mathrm{L}^{\ell}_{q}}\right](\mathrm{P})\right|^2 dS$$

$$+\sum_{\ell=1}^{L}\sum_{q=1}^{Q}\int_{\mathrm{C}_{\ell q}}\left|\boldsymbol{\nu}\times\left[\boldsymbol{E}_N^{\mathrm{U}^{\ell}_{q}}-\boldsymbol{E}_N^{\mathrm{L}^{\ell}_{Q+q-1}}\right](\mathrm{P})\right|^2 dS$$

$$+W^2\times(\text{previous three terms})\big|_{\boldsymbol{E}\text{ is replaced by }\boldsymbol{H}} \tag{33}$$

where $\Gamma^{\mathrm{U}}_{\ell q}$ and $\Gamma^{\mathrm{L}}_{\ell q}$ denote fictitious boundary segments in ℓ-th groove region (the horizontal dashed lines in Fig. 3, and $\mathrm{C}_{\ell q}$ is a segment of grating surface S_ℓ in one period which bounds U^{ℓ}_{q} and $\mathrm{L}^{\ell}_{Q-q+1}$. In addition, W is a proper weighting factor, for which an intrinsic impedance of vacuum is conventionally chosen.

4. NUMERICAL ANALYSIS

4.1. Discretization

Because computers cannot handle a continuous functions, we need to treat a finite number of sampled values of a function. Since (33) defines a least-squares problem in a function space, we first state how to discretize the problem.

Before doing this, let us modify the integrand terms of (33) slightly. We remove the common factor $\exp[i(\alpha x+\beta y)]$ from each function in the absolute value symbols. Thereby the resultant functions become periodic in X and Y with a period D. Bearing in mind that the rectangular rule gives the same result as the trapezoidal rule for a definite integral of a periodic function over one period, we apply the former rule to the modified (33).

We locate sampling points on the fictitious boundaries $\Gamma^{\mathrm{U}}_{\ell q}$ and $\Gamma^{\mathrm{L}}_{\ell q}$ ($\ell=1,\,2,\,\ldots,\,L;\ q=0,\,1,\,\ldots,\,Q-1$) and on the grating surface $\mathrm{C}_{\ell q}$ ($\ell=1,\,2,\,\ldots,\,L;\ q=1,\,2,\,\ldots,\,Q$). These are given by

$$(X,Y,Z)=\begin{cases}(x_i^{\mathrm{S}},y_j^{\mathrm{S}},z_q^{\ell}) & (i,j=1,\,2,\,\ldots,\,J_{\mathrm{S}};\ q=0,\,1,\,\ldots,\,Q)\\ (x_i^{\mathrm{C}},y_j^{\mathrm{C}},\eta_\ell(x_i^{\mathrm{C}},y_j^{\mathrm{C}})) & (i,j=1,\,2,\,\ldots,\,J_{\mathrm{C}})\end{cases} \tag{34}$$

The points x_i^{S}, y_j^{S}, x_i^{C}, and y_j^{C} are distributed with a fixed distance within the area $0<X<D$ and $0<Y<D$. Equation (34) represents $(Q+1)J_{\mathrm{S}}^2+J_{\mathrm{C}}^2$ points, on each of which we have four scalar boundary conditions, i.e., continuity of tangential electric and magnetic fields.

We determine the numbers J_{S} and J_{C} by the following rules:

- It is generally stated [9] that the number of lows of a Jacobian in the discretized least-squares problem, i.e., the number of linear equations in an over-determined set of equations, is twice as many as the number of columns:

$$(M_{\mathrm{T}} =)\ 4\{(Q+1)J_{\mathrm{S}}^2+J_{\mathrm{C}}^2\}L \approx 2\times 4L(2Q+1)(2N+1)^2\ (=2N_{\mathrm{T}}) \tag{35}$$

- The distance between two neighboring sampling points is fixed approximately:

$$\frac{J_{\mathrm{C}}^2}{J_{\mathrm{S}}^2} \approx \frac{\text{average area of } S_\ell \text{ in one period}}{D^2} \tag{36}$$

Solving (35) and (36) we obtain J_{S} and J_{C}.

Application of the rectangular rule to (33) gives

$$I_N \simeq I_{NJ} = ||\Phi\mathbf{A}-\mathbf{F}||_{M_{\mathrm{T}}}^2 \tag{37}$$

where $||\cdot||_{M_{\mathrm{T}}}$ denotes the M_{T}-dimensional Euclidean norm and Φ is a Jacobian having a block-diagonal structure

$$\Phi = \begin{bmatrix} \Phi_{00}^1 & \Phi_{01}^1 & 0 & \cdots & 0 \\ 0 & \Phi_{11}^1 & \Phi_{12}^1 & \ddots & \vdots \\ \vdots & \ddots & \ddots & \ddots & 0 \\ 0 & \cdots & 0 & \Phi_{QQ}^L & \Phi_{Q,Q+1}^L \end{bmatrix} \quad (M_{\mathrm{T}}\times N_{\mathrm{T}}) \tag{38}$$

Here, $\Phi_{qp}^\ell(\ell = 1,\ 2,\ \ldots,\ L;\ q = 0,\ 1,\ \ldots,\ Q;\ p = q,\ q+1)$ are $m_q^\ell \times n_p^\ell$ partial matrices. The elements of Φ_{qp}^ℓ are the modified boundary values of the modal functions at the sampling points. We assume that Φ is full rank ($\mathrm{rank}(\Phi) = N_{\mathrm{T}}$), i.e., the N_{T} column vectors of Φ are linearly independent.

The vectors $\mathbf{A}$ and $\mathbf{F}$ in (37) are related to the solution and excitation, respectively. See Appendix A for their detailed expressions.

4.2. A QR Method with SA

In solving a large problem where L (the number of grating boundaries), Q (the number of divisions), or N (the number of truncation) is increased, we employ the sequential accumulation (SA) [16] to reduce the computational complexity. The SA-scheme to obtain a QR decomposition of the Jacobian (38) is given in Appendix B, which is an extended version of the case of one-dimensional non-layered grating [12].

As a numerical check, we analyze the diffraction problem by non-layered doubly periodic deep grating shown in Fig. 1(b). Comparison of the conventional QR decomposition without SA and the new QR decomposition with SA is displayed Fig. 4. This shows the comparison of (a) memory size, (b) CPU time, and (c) computational cost (= memory size × CPU time). The angles θ, ϕ, and δ do not affect the displayed data and are not stated here. Computation was carried out on a 3.0 GHz personal computer with 1 GB memory. In employing SA, the memory size is reduced by $1/6\,(N=1)$ to $1/5\,(N=5)$; and the CPU time is reduced by 1/2 to 1/8. The computational cost, hence, is reduced by 1/12 to 1/40.

5. NUMERICAL RESULTS

5.1. Definition of Efficiencies and Errors

The diffraction efficiency of the (m, n)-th order propagating mode $(\mathrm{Re}(\gamma_{\ell mn}) \geq 0)$ is given by

(m, n)-th order reflection efficiency:

$$\rho_{mn} = \frac{\gamma_{0mn}}{\gamma_{000}} \cdot \left\{ \left| A_{1mn}^{\mathrm{TE}(0)} \right|^2 + \left| A_{1mn}^{\mathrm{TM}(0)} \right|^2 \right\} \tag{39}$$

(m, n)-th order transmission efficiency:

$$\tau_{mn} = \frac{\gamma_{Lmn}}{\gamma_{000}} \cdot \left\{ \left| D_{Lmn}^{\mathrm{TE}(0)} \right|^2 + \left| D_{Lmn}^{\mathrm{TM}(0)} \right|^2 \right\} \tag{40}$$

The energy error is defined by

$$\varepsilon_N = \left| 1 - {\sum_{m,n}}' \rho_{mn} - {\sum_{m,n}}' \tau_{mn} \right| \tag{41}$$

where $\sum'$ stands for the summation over the propagating orders. The energy error ε_N and the norm error on the boundary I_N, given by (B9), will be used in checking the accuracy of solutions.

5.2. Results of a Multilayered Singly Periodic Grating

We first show the results for the grating of Fig. 1(a). Figure 5 shows reflection efficiency as functions of the wavelength for the TE-mode $(\delta = 0^\circ)$ and the TM-mode $(\delta = 90^\circ)$ by the solid and dashed curves, respectively. Parameters in numerical computation are $Q = 3$ for both

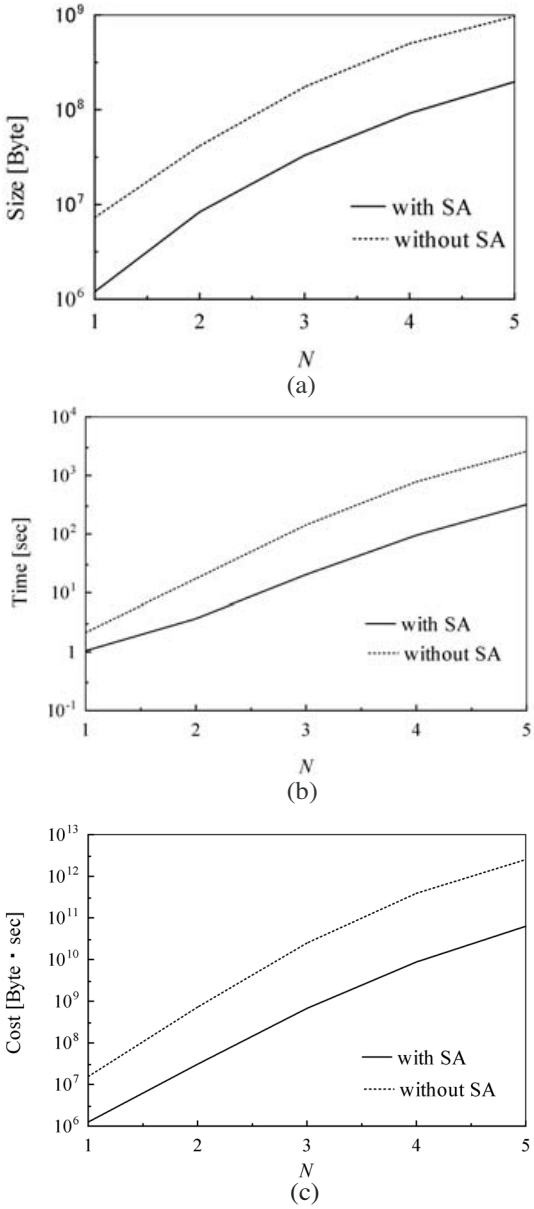

Figure 4. Comparison of the conventional QR decomposition without SA and the new QR decomposition with SA for a doubly periodic deep grating at $L = 1$ and $Q = 5$. The parameters are $2H_1/D = 1.0$, $n_0 = 1.0$, $n_1 = 2.0$, and $D/\lambda = 1.0$. (a) Memory size. (b) CPU time. (c) Computational cost.

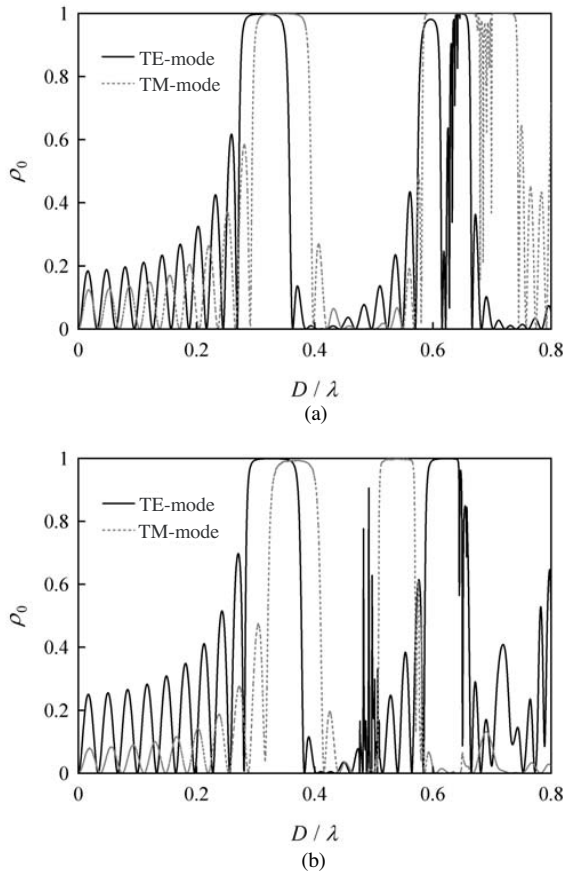

Figure 5. Reflection efficiency of multilayered grating as function of wavelength. The multilayer profile is given by: $2H_\ell/D = 0.4$, $L = 20$, $n_\ell = 1.0\,(\ell : \text{even})$, $= 2.0\,(\ell : \text{odd})$, $w_\ell/D = 0.5$, $p_\ell = 0^\circ\,(\ell : \text{odd})$, $= 180^\circ\,(\ell : \text{even})$. (a) $\theta = \phi = 0^\circ$. (b) $\theta = 30^\circ$ and $\phi = 0^\circ$.

modes, and $N = 15$ and 25 for the TE- and TM-modes, respectively. In the singly periodic case and $\phi = 0^\circ$, no mode conversion occurs. In both cases of polarization the normalized mean-square error I_N and the energy error ε_N are less than (a) 0.2% and (b) 1%.

In the TE-mode (TM-mode) case we observe a total reflection in the range (a) $D/\lambda = 0.29$ to 0.34 (0.30 to 0.38) and (b) $D/\lambda = 0.29$ to 0.36 (0.34 to 0.39). This agrees well with the photonic band gap predicted in [17]. But a common stop band in the TE-mode and the TM-mode does not appear from $\theta = 0^\circ$ to $\theta = 30^\circ$. This result had

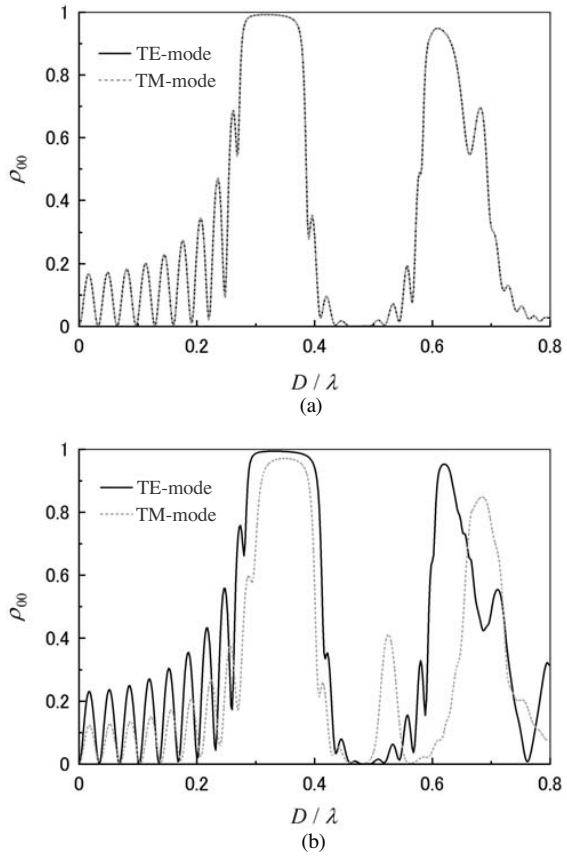

Figure 6. Reflection efficiency of multilayered doubly periodic grating as function of wavelength. The multilayer profile is given by: $2H_\ell/D = 0.4$, $L = 20$, $n_\ell = 1.0\,(\ell : \text{even}), = 2.0\,(\ell : \text{odd})$, $w_\ell/D = 0.5$, $p_\ell = 0^\circ\,(\ell : \text{odd}), = 180^\circ\,(\ell : \text{even})$. (a) $\theta = \phi = 0^\circ$. (b) $\theta = 30^\circ$ and $\phi = 0^\circ$.

been expected, because the polarization dependence is strong when the structure has periodicity in only one direction.

5.3. Results of a Multilayered Doubly Periodic Grating

We next show the results for the grating shown in Fig. 1(b). Figure 6 shows reflection efficiency by multilayered doubly periodic deep grating as functions of the wavelength. The solid curve and dashed curve represent the incidence of TE-mode ($\delta = 0^\circ$) and TM-mode ($\delta = 90^\circ$),

respectively. Parameters in numerical computation are $Q = 3$ and $N = 3$. The I_N and ε_N errors are both less than 1%.

In the TE-mode (TM-mode) we observe a total reflection in the range (a) $D/\lambda = 0.28$ to 0.37 (0.28 to 0.37) and (b) $D/\lambda = 0.3$ to 0.39 (0.32 to 0.38). The common stop band in the TE-mode and the TM-mode appears in the range $D/\lambda = 0.32$ to 0.37 from $\theta = 0^\circ$ to $\theta = 30^\circ$.

6. CONCLUSIONS

We have analyzed by Yasuura's method with a technique of extending the range of application for solving the problem of plane wave diffraction by the multilayered deep gratings. We first divided each grating region into some shallow horizontal layers. We then defined approximate solutions in each region in the form of truncated modal expansions. Remarkable reduction of the storage space requirement and CPU time in numerical computations was achieved by introducing a sequential accumulation. We have also confirmed that the common stop band appears in a certain wavelength range.

The present method can be used to elucidate a characteristic of photonic crystal and to design a crystal having desired complete gaps. As a future problem, we should attack the problem of eigenvalue to examine dispersion curves for multilayered deep gratings.

ACKNOWLEDGMENT

This work was supported in part by Grants-in-Aid for Scientific Research from Japan Society for the Promotion of Science (Grant number 17560313).

APPENDIX A. SOLUTION AND EXCITATION VECTORS

The solution vector $\mathbf{A}$ in (37) is defined by

$$\mathbf{A} = \left[\mathbf{A}_{10}^{\mathrm{T}}\ \mathbf{A}_{11}^{\mathrm{T}}\ \ldots\ \mathbf{A}_{\ell q}^{\mathrm{T}}\ \ldots\ \mathbf{A}_{LQ}^{\mathrm{T}}\ \mathbf{A}_{L,Q+1}^{\mathrm{T}}\right]^{\mathrm{T}} \quad (N_{\mathrm{T}} \times 1) \tag{A1}$$

where

$$\mathbf{A}_{10} = \left[\begin{array}{cc} A_{1mn}^{\mathrm{TE}(0)} & A_{1mn}^{\mathrm{TM}(0)} \end{array}\right]^{\mathrm{T}} \quad (n_0^1 \times 1) \tag{A2}$$

$$\mathbf{A}_{L,Q+1} = \left[\begin{array}{cc} D_{Lmn}^{\mathrm{TE}(0)} & D_{Lmn}^{\mathrm{TM}(0)} \end{array}\right]^{\mathrm{T}} \quad (n_{Q+1}^L \times 1) \tag{A3}$$

$$\mathbf{A}_{\ell q} = \left[A_{\ell mn}^{\mathrm{TE}(q)}\ A_{\ell mn}^{\mathrm{TM}(q)}\ B_{\ell mn}^{\mathrm{TE}(q)}\ B_{\ell mn}^{\mathrm{TM}(q)}\ C_{\ell mn}^{\mathrm{TE}(Q-q+1)}\right.$$
$$\left. C_{\ell mn}^{\mathrm{TM}(Q-q+1)}\ D_{\ell mn}^{\mathrm{TE}(Q-q+1)}\ D_{\ell mn}^{\mathrm{TM}(Q-q+1)}\right]^{\mathrm{T}}\ (n_q^\ell \times 1)$$
$$(\ell = 1, 2, \ldots, L; q = 1, 2, \ldots, Q) \tag{A4}$$

$$\mathbf{A}_{\ell 0} = \left[\ A_{\ell mn}^{\mathrm{TE}(0)}\quad A_{\ell mn}^{\mathrm{TM}(0)}\quad D_{\ell-1,mn}^{\mathrm{TE}(0)}\quad D_{\ell-1,mn}^{\mathrm{TM}(0)}\ \right]^{\mathrm{T}}\ (n_0^\ell \times 1)$$
$$(\ell = 2,\ 3,\ \ldots,\ L) \tag{A5}$$

The excitation vector in (37) is

$$\mathbf{F} = \left[\mathbf{f}_0^{1\,\mathrm{T}}\ \mathbf{f}_1^{1\,\mathrm{T}}\ \ldots\ \mathbf{f}_Q^{L\,\mathrm{T}}\right]^{\mathrm{T}} \quad (M_{\mathrm{T}} \times 1) \tag{A6}$$

where the first entry $\mathbf{f}_0^1$ consists of the sampled values of the incident wave i.e., $\left[-\boldsymbol{i}_z \times \mathbf{E}^{\mathrm{i}} \quad -\boldsymbol{i}_z \times \mathbf{H}^{\mathrm{i}}\right]$. Other subvectors $\mathbf{f}_q^\ell$ are m_q^ℓ-dimensional zero vectors.

APPENDIX B. QR METHOD WITH SA

The procedure is composed of sequential steps as follows.

$$\begin{array}{llll} 1-0, & 1-1, & \ldots, & 1-Q, \\ 2-0, & 2-1, & \ldots, & 2-Q, \\ \cdots & \cdots & \cdots & \cdots \\ L-0, & L-1, & \ldots, & L-Q, \quad L-(Q+1) \end{array}$$

Each step is described as follows.

- Step $1-0$:
  We pick out the partial matrices Φ_{00}^1 and Φ_{01}^1 from Φ, as well as the corresponding element $\mathbf{f}_0^1$ in the right-hand side, to define

$$\Phi^{(10)} = \left[\ \Phi_{00}^1 \quad \Phi_{01}^1\ \right](m_0^1 \times (n_0^1 + n_1^1)), \quad \mathbf{f}^{(10)} = \left[\ \mathbf{f}_0^1\ \right] \quad (m_0^1 \times 1) \tag{B1}$$

  We then decompose $\Phi^{(10)}$ to obtain

$$\Phi^{(10)} = \mathrm{Q}^{(10)}\widetilde{\mathrm{R}}^{(10)} = \mathrm{Q}^{(10)} \left[\begin{array}{cc} \mathrm{R}_{00}^{1(10)} & \mathrm{R}_{01}^{1(10)} \\ 0 & \mathrm{R}_{11}^{1(10)} \\ \hline 0 & \end{array}\right] \tag{B2}$$

  where the symbols Q and R are used to express a unitary and an upper triangular matrices, respectively. Hence, if we

operate $\mathrm{Q}^{(10)*}$ ($= \overline{\mathrm{Q}^{(10)\mathrm{T}}}$, where the asterisk and overline denote inverse and complex conjugation, respectively) to a combination $[\Phi^{(10)}\ \mathbf{f}^{(10)}]$ from the left, we arrive at

$$\mathrm{Q}^{(10)*}\left[\begin{array}{cc|c} \Phi^{(10)} & & \mathbf{f}^{(10)} \end{array}\right] = \left[\begin{array}{cc|c} \mathrm{R}_{00}^{1(10)} & \mathrm{R}_{01}^{1(10)} & \mathbf{g}_0^{1(10)} \\ 0 & \mathrm{R}_{11}^{1(10)} & \mathbf{g}_1^{1(10)} \\ \hline 0 & & \mathbf{e}^{(10)} \end{array}\right] \tag{B3}$$

- Step $\ell - q$ ($\ell = 1, 2, \ldots, L;\ q = 1, 2, \ldots, Q$):
  We pick out the partial matrices $\mathrm{R}_{qq}^{\ell(\ell,q-1)}$ from $\widetilde{\mathrm{R}}^{(\ell,q-1)}$, Φ_{qq}^{ℓ} and $\Phi_{q,q+1}^{\ell}$ from Φ, $\mathbf{g}_q^{\ell(\ell,q-1)}$, and $\mathbf{f}_q^{\ell}$ to define

$$\begin{aligned} \Phi^{(\ell q)} &= \begin{bmatrix} \mathrm{R}_{qq}^{\ell(\ell,q-1)} & 0 \\ \Phi_{qq}^{\ell} & \Phi_{q,q+1}^{\ell} \end{bmatrix} \ ((n_q^{\ell} + m_q^{\ell}) \times (n_q^{\ell} + n_{q+1}^{\ell})), \\ \mathbf{f}^{(\ell q)} &= \begin{bmatrix} \mathbf{g}_q^{\ell(\ell,q-1)} \\ \mathbf{f}_q^{1} \end{bmatrix} \ ((n_q^{\ell} + m_q^{\ell}) \times 1) \end{aligned} \tag{B4}$$

  We obtain $\mathrm{Q}^{(\ell q)}\widetilde{\mathrm{R}}^{(\ell q)}$ by decomposing $\Phi^{(\ell q)}$. Then, operating $\mathrm{Q}^{(\ell q)*}$ to $[\Phi^{(\ell q)}\ \mathbf{f}^{(\ell q)}]$, we arrive at

$$\Phi^{(\ell q)} = \mathrm{Q}^{(\ell q)}\widetilde{\mathrm{R}}^{(\ell q)} = \mathrm{Q}^{(\ell q)} \left[\begin{array}{cc} \mathrm{R}_{qq}^{\ell(\ell q)} & \mathrm{R}_{q,q+1}^{\ell(\ell q)} \\ 0 & \mathrm{R}_{q+1,q+1}^{\ell(\ell q)} \\ \hline 0 & \end{array}\right] \tag{B5}$$

$$\mathrm{Q}^{(\ell q)*}\left[\begin{array}{cc|c} \Phi^{(\ell q)} & & \mathbf{f}^{(\ell q)} \end{array}\right] = \left[\begin{array}{cc|c} \mathrm{R}_{qq}^{\ell(\ell q)} & \mathrm{R}_{q,q+1}^{\ell(\ell q)} & \mathbf{g}_q^{\ell(\ell q)} \\ 0 & \mathrm{R}_{q+1,q+1}^{\ell(\ell q)} & \mathbf{g}_{q+1}^{\ell(\ell q)} \\ \hline 0 & & \mathbf{e}^{(\ell q)} \end{array}\right] \tag{B6}$$

- Step $\ell - 0$ ($\ell = 2, 3, \ldots, L$):
  We pick out the partial matrices $\mathrm{R}_{Q+1,Q+1}^{\ell-1(\ell-1,Q)}$ from $\widetilde{\mathrm{R}}^{(\ell-1,Q)}$, Φ_{00}^{ℓ} and Φ_{01}^{ℓ} from Φ, $\mathbf{g}_{Q+1}^{\ell-1(\ell-1,Q)}$, and $\mathbf{f}_0^{\ell}$ to define

$$\begin{aligned} \Phi^{(\ell 0)} &= \begin{bmatrix} \mathrm{R}_{Q+1,Q+1}^{\ell-1(\ell-1,Q)} & 0 \\ \Phi_{00}^{\ell} & \Phi_{01}^{\ell} \end{bmatrix} \ ((n_0^{\ell} + m_0^{\ell}) \times (n_0^{\ell} + n_1^{\ell})), \\ \mathbf{f}^{(\ell 0)} &= \begin{bmatrix} \mathbf{g}_{Q+1}^{\ell-1(\ell-1,Q)} \\ \mathbf{f}_0^{\ell} \end{bmatrix} \ ((n_0^{\ell} + m_0^{\ell}) \times 1) \end{aligned} \tag{B7}$$

We obtain $\mathrm{Q}^{(\ell 0)}\widetilde{\mathrm{R}}^{(\ell 0)}$ by decomposing $\Phi^{(\ell 0)}$. Then, operating $\mathrm{Q}^{(\ell 0)*}$ to $[\Phi^{(\ell 0)}\ \mathbf{f}^{(\ell 0)}]$, we again arrive at (B5) and (B6) with q replaced by 0.

- Step $L-(Q+1)$:
  Once $\mathrm{R}_{qq}^{\ell(\ell q)}$, $\mathrm{R}_{q,q+1}^{\ell(\ell q)}$ and $\mathbf{g}_q^{\ell(\ell q)}$ are obtained, the solution vectors $\mathbf{A}_{\ell q}$ are found by solving simultaneous linear equations, which are constructed from upper triangular submatrices only, by backward substitution:

$$\begin{cases} \mathrm{R}_{Q+1,Q+1}^{L(LQ)}\mathbf{A}_{L,Q+1} = \mathbf{g}_{Q+1}^{L(LQ)} \\ \mathrm{R}_{QQ}^{L(LQ)}\mathbf{A}_{LQ} = \mathbf{g}_Q^{L(LQ)} - \mathrm{R}_{Q,Q+1}^{L(LQ)}\mathbf{A}_{L,Q+1} \\ \mathrm{R}_{qq}^{\ell(\ell q)}\mathbf{A}_{\ell q} = \mathbf{g}_q^{\ell(\ell q)} - \mathrm{R}_{q,q+1}^{\ell(\ell q)}\mathbf{A}_{\ell,q+1} \\ \quad (\ell = L, L-1, \ldots, 1;\ q = Q-1, Q-2, \ldots, 0) \\ \mathrm{R}_{QQ}^{\ell(\ell Q)}\mathbf{A}_{\ell Q} = \mathbf{g}_Q^{\ell(\ell Q)} - \mathrm{R}_{Q,Q+1}^{\ell(\ell Q)}\mathbf{A}_{\ell+1,0} \quad (\ell \neq L;\ q = Q) \end{cases} \tag{B8}$$

The above is an algorithm of QR method with SA. We can prove that the solution vector $\mathbf{A}$, which is composed of the vectors $\mathbf{A}_{\ell q}$ obtained from (B8), agrees with the solution vector found by the conventional QR method. The minimized error is given by

$$\begin{aligned} I_{NJ\min} \;=\; & ||\mathbf{e}^{(10)}||^2_{m_0^1-(n_0^1+n_1^1)} + \sum_{\ell=1}^{L}\sum_{q=1}^{Q-1}||\mathbf{e}^{(\ell q)}||^2_{m_q^\ell - n_{q+1}^\ell} \\ & + \sum_{\ell=2}^{L}||\mathbf{e}^{(\ell 0)}||^2_{m_0^\ell - n_1^\ell} + \sum_{\ell=1}^{L-1}||\mathbf{e}^{(\ell Q)}||^2_{m_Q^\ell - n_0^{\ell+1}} \\ & + ||\mathbf{e}^{(LQ)}||^2_{m_Q^L - n_{Q+1}^L} \end{aligned} \tag{B9}$$

REFERENCES

1. Yablonovitch, E., "Inhibited spontaneous emission in solidstate physics and electronics," *Phys. Rev. Lett.*, Vol. 58, 2059–2062, 1987.
2. Ho, K. M., C. T. Chan, and C. M. Soukoulis, "Existence of a photonic gap in periodic dielectric structures," *Phys. Rev. Lett.*, Vol. 65, 3152–3155, 1990.
3. Villeneuve, P. and M. Piche, "Photonic band gaps in two dimensional square and hexagonal lattices," *Phys. Rev. B*, Vol. 46, 4969–4972, 1992.

4. Yasuura, K. and T. Itakura, "Approximation method for wave functions," *Kyushu Univ. Tech. Rep.*, Vol. 38, No. 1, 72–77, 1965.
5. Yasuura, K. and T. Itakura, "Complete set of wave functions," *Kyushu Univ. Tech. Rep.*, Vol. 38, No. 4, 378–385, 1966.
6. Yasuura, K. and T. Itakura, "Approximate algorism by complete set of wave functions," *Kyushu Univ. Tech. Rep.*, Vol. 39, No. 1, 51–56, 1966.
7. Yasuura, K., "A view of numerical methods in diffraction problems," *Progress in Radio Science*, W. V. Tilson and M. Sauzade (eds.), 1966–1969, 257–270, URSI, Brussels, 1971.
8. Ikuno, H. and K. Yasuura, "Improved point-matching method with application to scattering from a periodic surface," *IEEE Trans. Antennas Propagat.*, Vol. AP-21, No. 5, 657–662, 1973.
9. Davies, J. B., "A least-squares boundary residual method for the numerical solution of scattering problems," *IEEE Trans., Microwave Theory Tech.*, Vol. MTT-21, No. 2, 99–104, 1973.
10. Van den Berg, P. M., "Reflection by a grating: Rayleigh methods," *J. Opt. Soc. Am.*, Vol. 71, No. 10, 1224–1229, 1981.
11. Hugonin, J. P., R. Petit, and M. Cadilhac, "Plane-wave expansions used to describe the field diffracted by a grating," *J. Opt. Soc. Am.*, Vol. 71, No. 5, 593–598, 1981.
12. Ohtsu, M., Y. Okuno, A. Matsushima, and T. Suyama, "A combination of up- and down-going floquet modal functions used to describe the field inside grooves of a deep grating," *Progress In Electromagnetics Research*, PIER 64, 293–316, 2006.
13. Chen, C. C., "Transmission of microwave through perforated flat plates of finite thickness," *IEEE Trans., Microwave Theory Tech.*, Vol. MTT-21, 1–6, 1973.
14. Matsuda, T. and Y. Okuno, "A numerical analysis of planewave diffraction from a multilayer-overcoated grating," *IEICE*, Vol. J76-C-I, No. 6, 206–214, 1993.
15. Matsuda, T. and Y. Okuno, "Numerical evaluation of plane-wave diffraction by a doubly periodic grating," *Radio Sci.*, Vol. 31, No. 6, 1791–1798, 1996.
16. Lawson, C. L. and R. J. Hanson, *Solving Least-Squares Problems*, Prentice-Hall, Englewood Cliffs, NJ, 1974.
17. Tan, W.-C., T. W. Preist, J. R. Sambles, M. B. Sobnack, and N. P. Wanstall, "Calculation of photonic band structures of periodic multilayer grating systems by use of a curvilinear coordinate transformation," *J. Opt. Soc. Am. A*, Vol. 15, No. 9, 2365–2372, 1998.